Title: Emergence of an adaptive command for orienting behavior in premotor brainstem neurons of barn owls

Abbreviated title: Adaptive motor command from the readout of a sensory map

Authors: Fanny Cazettes[1,2], Brian J. Fischer[3], Michael V. Beckert[1], Jose L. Pena[1*]

Affiliations: [1]Dominick P Purpura Department of Neuroscience, Albert Einstein College of Medicine, New York 10461, USA

[2]Champalimaud Neuroscience Programme, Champalimaud Center for the Unknown, 1400-038, Lisbon, Portugal

[3] Department of Mathematics, Seattle University, Seattle, Washington, 98122, USA

Corresponding author: Jose L. Pena. Dominick P Purpura Department of Neuroscience, Albert Einstein College of Medicine, 1410 Pelham Parkway South, Bronx, New York, 10461, USA

jose.pena@einstein.yu.edu

Number of pages: 37

Number of figures: 5

Number of words for Abstract: 175

Number of words for Introduction: 548

Number of words for Discussion: 926

Conflict of interest: The authors declare no competing financial interests.

Acknowledgements: This work was funded by NIH grants DC012949 and DC007690. We thank Kourosh Saberi for providing the data used in Fig. 4A and Adam Kohn for comments on

the manuscript. Clifford Keller helped hand-raise the owlets and Daniel Munch participated in the blind analysis of behavior.

Abstract: The midbrain map of auditory space commands sound-orienting responses in barn owls. Owls precisely localize sounds in frontal space but underestimate the direction of peripheral sound sources. This bias for central locations was proposed to be adaptive to the decreased reliability in the periphery of sensory cues used for sound localization by the owl. Understanding the neural pathway supporting this biased behavior provides a means to address how adaptive motor commands are implemented by neurons. Here we find that the sensory input for sound direction is weighted by its reliability in premotor neurons of the owl's midbrain tegmentum such that the mean population firing rate approximates the head-orienting behavior. We provide evidence that this coding may emerge through convergence of upstream projections from the midbrain map of auditory space. We further show that manipulating the sensory input yields changes predicted by the convergent network in both premotor neural responses and behavior. This work demonstrates how a topographic sensory representation can be linearly read out to adjust behavioral responses by the reliability of the sensory input.

Significance statement: This research shows how statistics of the sensory input can be integrated into a behavioral command by readout of a sensory representation. The firing rate of midbrain premotor neurons receiving sensory information from a topographic representation of auditory space is weighted by the reliability of sensory cues. We show that these premotor responses are consistent with a weighted convergence from the topographic sensory representation. This convergence was also tested behaviorally, where manipulation of stimulus

properties led to bidirectional changes in sound localization errors. Thus a topographic representation of auditory space is translated into a premotor command for sound localization that is modulated by sensory reliability.

INTRODUCTION

The synthesis of motor commands weighted by sensory reliability is critical for understanding adaptive behavior. To address this question, we investigated the neural basis of the centrality bias of barn owls, which is a systematic underestimation of sound sources towards the center of gaze (Hausmann et al., 2009; Knudsen et al., 1979). This centrality bias may be optimal for the owl's prey capture, where the amount of bias reflects the relative weight given to sensory evidence depending on the reliability of the sensory input (Fischer and Pena, 2011; Girshick et al., 2011; Schwartz et al., 2007). Yet, the neural circuit decoding a behavioral command that integrates the reliability of sensory evidence has not been demonstrated. This study describes how such a command may emerge in a premotor neural population that controls orienting behaviors in the sound localization system of the owl.

Most animals use interaural time difference (ITD) for inferring the horizontal direction of sound location (Strutt, 1907; Blauert, 1997). In the barn owl, a map of auditory space emerges in the external nucleus of the inferior colliculus (ICx) (Knudsen and Konishi, 1978), where selectivity for ITD determines the horizontal spatial tuning of auditory neurons. The ICx map is a distorted representation of space where the front is overrepresented (Knudsen, 1982)(Figure 1). Additionally, frequency and spatial selectivity of ICx neurons co-vary (Cazettes et al., 2014), where neurons preferring frontal directions are tuned to higher frequencies than peripheral neurons (Figure 1). This direction-dependent frequency selectivity corresponds to how the

variability of interaural phase difference changes across frequency and direction, estimated from the owl's head-related transfer function (Cazettes et al., 2014). Previous studies have proposed that this non-uniform spatial and frequency selectivity across the ICx allows for the representation of ITD reliability (Fischer and Pena, 2011; Rich et al., 2015; Cazettes et al., 2016).

ICx projects point-to-point to the optic tectum (OT), analog of mammalian superior colliculus (Knudsen and Knudsen, 1983), leading to both structures having neurons with similar spatial and frequency tunings (Olsen et al., 1989; Knudsen, 1984). As a result, both ICx and OT display similar maps of auditory space, here referred to as the space-map (Figure 1). OT projects to the midbrain tegmentum (mTeg), which drives the spinal-cord motoneurons that generate the head-orienting response to sound (Masino and Knudsen, 1992, 1993) (Figure 1). In vertebrates, the tectotegmental pathway contributes prominently to the generation of orienting movements of the eyes, head, and body (Masino, 1992; du Lac and Knudsen, 1990). Anatomical studies of the tectotegmental projections in the barn owl suggest that the topographic representation of space in the OT is translated into a representation of orthogonal movement vectors in mTeg (Masino and Knudsen, 1990, 1992, 1993).

This study examined whether responses of premotor neurons in mTeg match the owl's sound localizing behavior, how these responses emerge, and whether they reflect the reliability of the sensory input. We found the mean population response in mTeg matches the owl's behavior, and could be explained by a convergence from OT to mTeg. Furthermore, both the mTeg responses and orienting bias of behaving owls changed with manipulations of the sensory reliability and sound frequency in a consistent manner. Thus, we provided evidence of a neural network that weights sensory input by its reliability to encode an adaptive behavioral command.

MATERIALS & METHODS

Electrophysiology

Surgical procedure: Surgery was performed as described previously (Wang et al., 2012). Briefly, adult American barn owls (*Tyto furcata*; 3 females and 3 males; ages 3 to 5 years old) were anesthetized with intramuscular injections of ketamine hydrochloride (Ketaset; 20 mg/kg, intramuscular) and xylazine (Anased; 4 mg/kg, intramuscular). Prophylactic antibiotics (ampicillin; 20 mg/kg, intramuscular) and lactated Ringer's solution (10 ml, subcutaneous) were injected at the beginning of each session. An analgesic, carprofen (Rimadyl; 3mg/kg, intramuscular), was administered at the end of each session to prevent inflammation and pain. These procedures complied with National Institutes of Health and guidelines of the Albert Einstein College of Medicine's Institute of Animal Studies.

Recording from awake animals was impractical in these experiments as electrophysiology required serial electrode penetrations, head restraint, and long recording sessions (up to 10 hours). To control for varying levels of anesthesia, records of the time of each recording relative to anesthetic administration were rigorously maintained. Experiments were interrupted if first-spike latencies or response thresholds changed. Regardless, the effect of anesthesia in the midbrain has been shown to be less pronounced than in the forebrain (Ter-Mikaelian et al., 2007; Schumacher et al., 2011) and therefore lessens concerns about changes in neural response under anesthesia.

Extracellular recordings of ICx, OT and mTeg neurons: Single-unit responses were recorded using 1MΩ tungsten electrodes (A-M Systems; Carlsborg, WA). Tucker Davis Technologies (TDT; Alachua, FL) System 3 and custom written Matlab software (Mathworks) were used to record neural data. ICx and OT were located stereotaxically and confirmed by the characteristic

113 responses to ITD and interaural level difference and firing properties (Wang et al., 2012). The
114 mTeg was also located stereotaxically (Masino and Knudsen, 1992, 1993) but recording from
115 this structure was further verified with microstimulation (see below).

116 *Microstimulation:* Recordings in mTeg were confirmed with microstimulation. At the end of
117 each recording, microstimulation at the recording site was conducted to verify that eye
118 movements were elicited and that the same electrical stimulus was no longer able to elicit eye
119 movements when the electrode was moved a few hundred micrometers away from the recording
120 site. A programmable digital stimulator (WPI, DS8000) was used to deliver trains of current
121 pulses (5ms pulse width, 200Hz, 80ms duration) through the recording electrode, varying the
122 current amplitude from 50 to 150 μA with inter-stimulus intervals larger than 15 seconds (as
123 described in Netser et al., 2010). In most experiments, 130 μA or less was enough to induce
124 unequivocal eye movements.

125 **Sound stimulation**

126 All experiments were performed inside a double-walled sound-attenuating chamber. Custom-
127 made earphones consisting of a calibrated speaker (Knowles model 1914) and a microphone
128 (Knowles model EK-23024) were inserted in the owl's ear canal (Wang et al., 2012). Auditory
129 stimuli delivered through the earphones consisted of 100 to 150 ms signals with a 5 ms rise-fall
130 time at 10-20 dB above threshold. For each ICx, OT, and mTeg neuron, we first measured the
131 ITD and rate-level responses with broadband noise (0.5 – 10 kHz). ITD was initially varied from
132 ±300 μs with 30 μs steps over 5-10 trials for ICx and OT and 20 trials for mTeg. Sound level
133 varied from 0 dB SPL to 70 dB SPL in 5-dB steps. Frequency tuning was measured with tones
134 ranging from 500 Hz to 8000 Hz varied in 200 to 500 Hz steps over 20 trials. Neural responses to

ITD in mTeg were also recorded at various frequencies (from 1 to 6 kHz, 1 kHz steps, same ITD protocol as broadband). Stimuli within all tested ranges were randomized during data collection.

To manipulate the binaural correlation (BC), three random noise signals (N1, N2, and N3) were generated. N1 was delivered to one ear and its copy with a time shift, to produce an ITD, was delivered to the other ear. N2 and N3 were added to the N1 in the left and right ear respectively. These additional noise signals reduced the correlation between the signals in the two ears, depending on the relative amplitudes of the uncorrelated and correlated noises. Binaural correlation was calculated from $BC = 1/(1 + k^2)$, where k is the ratio between the root-mean-square amplitudes of the uncorrelated and correlated noises (Saberi et al., 1998). On a subset of ICx neurons (n=46) and on all recorded mTeg neurons, we obtained ITD curves (±300 µs; 30 µs steps; 20 repetitions) using noise bursts at different BCs (from 0 [noise in each ear is independent] to 1 [noise in each ear is the same], in 0.2 steps).

Finally, for all mTeg neurons we measured ITD curves (±300 µs; 30 µs steps; 20 repetitions) with low (500-3500 Hz) and high (4500-7500 Hz) frequency band-pass sounds as well as broadband noise (500-9000 Hz).

Behavior

Remote eye tracking: Eye movements triggered by microstimulation in mTeg were measured with high-speed video imaging using a commercially available eye tracking system (EyeLink 1000) that detected the pupil and the position of the corneal reflection. Eyelids were opened momentarily to conduct the test after each recording using a custom made retractor. This procedure and the anesthesia did not prevent blinking of the nictitating membrane, allowing for natural protection of the eyes from drying.

157 *Head-orienting behavior:* Head-orienting behavior to sound was measured for three hand-raised
158 barn owls only trained to stand on a perch at the center of a speaker array. The speaker array
159 consisted of an azimuthal linear array of 21 speakers, a subset of a hemispherical array of
160 speakers constructed inside a sound-attenuating chamber (Wang et al., 2012; Cazettes et al.,
161 2014). The linear array spanned 100 degrees to the left and right of the midline, with 10 degrees
162 separation between speakers. Each speaker was calibrated in place using a microphone mounted
163 on a pan-tilt robot located at the array center. Head saccades were recorded with a pair of high-
164 speed infrared cameras (Fastec Imaging, 100 frames per sec) mounted in the corners of the room.
165 Head saccades were then tracked using custom designed image-analysis code (Xcitec,
166 Proanalyst) from images calibrated in 3-D using a grid located at the same position of the owl's
167 head. Owls were presented with the same noise bursts used to measure neural responses (100 ms
168 long, 5 ms rise-fall time, high and low frequency band-pass sounds, and broadband-noise) but
169 through this free-field array. The setup allowed us to measure head saccades from any starting
170 head position, which made it possible to rule out positional biases. To account for the position of
171 the animal in the field of view of the cameras, the owl's perch was designed such that it only
172 allowed the bird a single stance. However, owls did not always look straight ahead when the
173 stimulus was presented; therefore, the measured angles of head turn were transformed into a
174 head-centered coordinate system. Owls were unrewarded in this task to avoid biases introduced
175 by training. For each sound presentation, the frequency band (0.5-3.5 kHz, 4.5-7.5 kHz or 0.5-9
176 kHz) and location (±100 deg, 10 deg separation) of the source were randomized by the software.
177 The experimenter initiated a trial when the owl was standing upright and its beak (the tracking
178 reference) was in the field of view of both cameras. The experimenter remained blind to the
179 properties of the sound.

180 **Experimental Design and Statistical Analysis**

181 No significant differences between sexes were observed in neural responses; therefore data from
182 the two groups were pooled.

183 *Electrophysiological data*: For each stimulus parameter, a rate curve was computed by averaging
184 the firing rate during sound stimulation over trials. The spontaneous firing rate, obtained when
185 no sound stimulation was presented, was subtracted from the response to the stimulus. Best ITDs
186 were defined as the center of the range that elicited 50% of the maximum response of each
187 tuning-curve. To assess the relative broadness of the frequency tuning we calculated the areas
188 under the normalized frequency tuning curves. To find the peak of ITD-tuning curves of mTeg
189 neurons to tonal stimulation we first fitted the curves with a cosine function. We then defined the
190 ITD corresponding to the closest maximum from 0 μs as the peak (Cazettes et al., 2014). The
191 changes of ITD tuning with BC were consistent in both hemispheres (maximal changes for sound
192 directions within the contralateral hemifields). Thus, analyses of the mean mTeg response were
193 performed on the combined data, normalized to contralateral and ipsilateral side leading.

194 ITD increases with eccentricity (Moiseff, 1989): small values of ITD (~0 μs) are associated with
195 frontal directions and larger values of ITD (~200 μs) are associated with the periphery. Thus, we
196 converted ITD to azimuth (Moiseff, 1989) to measure the bias predicted by the mTeg response to
197 ITD.

198 *Behavioral data*: Behavioral experiments used three different owls, two females and one male.
199 Head orientation and angular velocity were computed offline using image-analysis software
200 (Xcitec, Proanalyst). Individuals analyzing the data remained blind to the location of the sound
201 source until the end. Subsets of the data were analyzed independently by different persons to
202 confirm the analysis was consistent across individuals. Trials where the owls' bodies moved

during the presentation of the stimulus or where the beak disappeared from the field of view of the cameras were discarded. Head movements could be classified as rotation, translation, or fixation, based on angular velocity (Ohayon et al., 2006). Saccades were defined as head rotations with an angular velocity greater than 50 deg.sec^{-1} (Knudsen et al., 1979; du Lac and Knudsen, 1990; Ohayon et al., 2006). When translational movements were included in the analysis the results remained consistent, albeit more variable. We measured saccade latencies as the time from the onset of each presentation of a stimulus to the first video frame where the owl's head started rotating. Median latency varied across animals (owl L=240 ms; owl F=520 ms; owl P=210 ms). These values are higher than previous reports (Hausmann et al., 2009; du Lac and Knudsen, 1990; Knudsen et al., 1979). The shorter response latency may be attributed to both the motivational and anticipatory state of the owls as most previous studies were conducted with trained owls that were rewarded if the saccade was correct. For each owl, there was no significant difference between the latencies across stimulus conditions (Wilcoxon rank-sum test, $p = 0.98$). Saccades whose latency was greater than 1 sec were discarded. The criteria for classifying movements as saccades became unreliable when the sound source was close to the front (Knudsen et al., 1979; Hausmann et al., 2009), therefore only head-turns evoked by sources located >10 degrees away from the initial head angle were included in the analysis.

Modeling

Heterogeneous population of neurons in the space-maps: We modeled a space-map population of 500 neurons. To incorporate the overrepresentation of frontal space into the modeled population, the density of preferred direction X was drawn from a Laplace prior:

$$p(X) \propto \exp\left(-\frac{|X|}{b}\right)$$

225 where the scale parameter is *b*=25 (Fischer and Pena, 2011; Knudsen, 1982). First, broadband
226 noise signals between 0.2 and 12 kHz were passed through a gammatone filter-bank with center
227 frequencies ranging from 0.25 kHz to 8 kHz in 0.25 kHz steps. The time constants of the filters
228 were specific to the owl and estimated from Koppl (1997) to model cochlear filters, as described
229 in Fischer et al. (2009). The outputs were cross-correlated and transformed by an exponential
230 input-output function to produce a set of frequency-dependent ITD curves (from 0.5 to 8 kHz).
231 The input to ICx was modeled as a weighted sum of the frequency-dependent ITD curves. The
232 weights were varied with direction to model the direction-dependent frequency tuning in ICx
233 (Cazettes et al., 2014). The weights for each neuron have a Gaussian shape with a center and
234 width selected to match the observed frequency tuning at the preferred direction of the neuron.
235 The weighted sum of the frequency-dependent ITD curves was passed through an exponential
236 nonlinearity to produce the firing rates of Poisson neurons that modeled ICx responses. The
237 responses in OT, which receive point-to-point projections from ICx (Knudsen and Knudsen,
238 1983), are influenced by feedback inhibition that serves to select the dominant stimulus when
239 multiple peaks of activity are present in the map (Mysore and Knudsen, 2012, 2014). To model
240 OT neurons, we used a simplified version of the model of Mysore and Knudsen (2012, 2014) by
241 multiplying the ICx activity pattern by a rectangular window function to select the dominant
242 peak. The window takes a value of one on an interval that is 28 degrees wide centered at the
243 location of the peak in a smoothed version of the ICx activity pattern. The decoding analyses
244 were applied to the windowed response pattern representing the population activity of the OT.

245 We hypothesized that a linear transformation of the OT population responses could explain the
246 tunings of neurons in mTeg. Under this hypothesis the mTeg response to ITD should be
247 explained entirely as a linear combination of ITD-tuning curves from OT. Therefore, we

modeled the responses in mTeg with a weighted sum of the OT population. To estimate the weights of the convergence, we used discrete Fourier transforms (FFT) of the experimental mTeg ITD tuning curves calculated after offsetting the curves to zero mean, as described previously (Vonderschen and Wagner, 2012). The weights given by the normalized FFT phase spectra of mTeg neurons were applied to OT neurons with equivalent preferred frequency. The modeled mTeg response was therefore given by

$$Y_i(ITD) = \sum_{n=1}^{N} f_{i,n} X_n(ITD)$$

where $X_n(ITD)$ is the modeled ITD curve of the nth neuron in OT and $f_{i,n}$ the weights given by the FFT phase spectra of the ith mTeg neurons at the preferred frequency of the nth OT neuron.

RESULTS

ITD tuning in mTeg

To assess the spatial tuning of premotor neurons downstream of the space-maps (i.e, ICx and OT), we conducted single-unit recording of auditory responses in mTeg using metal electrodes. Previous studies have shown that microstimulation of mTeg produces head-orienting responses and eye-movements (Masino and Knudsen, 1993), and that this method could be used to reliably identify this region. Although these studies were successful in establishing mTeg as a region that commands orienting behaviors, sound-evoked responses of these neurons were never explored. To target mTeg we used the same stereotaxic (Masino and Knudsen, 1992, 1993) and microstimulation (Masino and Knudsen, 1990, 1993; Netser et al., 2010) guidelines reported previously. For each recording site, it was verified that: 1) microstimulation at the recording site

elicited micro-saccades (Figure 2A,B) and 2) that microstimulation with the same current intensity no longer elicited saccades after the electrode was moved a few hundred microns away from the recording site.

Like ICx and OT neurons, mTeg neurons were tuned to ITD. For tonal stimulation, ITD curves in both ICx (Figure 2C) and mTeg (Figure 2D) were periodic, as previously reported in OT (Saberi et al., 1999). However, when broadband noise was used, a notable difference was observed. Unlike neurons in ICx, which display ITD curves for broadband noise with a narrow larger peak flanked by smaller side peaks (Takahashi and Konishi, 1986) (Figure 2E), all mTeg neurons stimulated with broadband noise ($n = 36$) displayed ITD tuning favoring the contralateral hemifield (one exemple neuron is plotted in Figure 2F). The maxima of these broadband-noise tuning curves were away from the midline on the contralateral side. Although in some neurons there was a slight response decrease at eccentric directions (ITD > 100 μs), in the population average this decrease was not statistically significant from the maximum response ($F(6,245) = 0.34$, $p = 0.92$, ANOVA), and thus the general population response in mTeg may be viewed as quasi-sigmoidal.

Emergence of mTeg tuning

We tested whether the ITD tuning of mTeg neurons was consistent with a convergent projection from OT to mTeg, as proposed for the midbrain network guiding eye saccades (Groh, 2001). If mTeg neurons received convergent input across the space-map from OT, their responses should reflect the varying ITD and frequency selectivity of OT neurons previously observed (Knudsen, 1984; Cazettes et al., 2014) (Figure 1). To test this hypothesis, we investigated two specific predictions for the convergence from OT to mTeg on auditory responses: 1) because frequency tuning varies across the space-map (Cazettes et al., 2014; Knudsen, 1984), a downstream neuron

292 receiving convergent input from OT should have broader frequency tuning; and 2) because
293 preferred ITD co-varies with preferred frequency in ICx and OT (Cazettes et al., 2014; Knudsen,
294 1984), stimulation with tones will drive activity in only a subset of the cells exciting each mTeg
295 neuron. Thus, convergence from OT to mTeg predicts that mTeg neurons should prefer more
296 frontal ITDs for high frequency sounds and more peripheral ITDs for low frequency sounds.

297 To test the prediction of broader frequency tuning in mTeg, we measured the half-width of
298 frequency tuning curves in ICx, OT, and mTeg neurons. Frequency tuning curves were
299 significantly broader in mTeg than in ICx and OT neurons (Figure 2G,H, mean ± s.d difference
300 in frequency bandwidth: 2.4 kHz ± 0.3 kHz, Wilcoxon rank-sum test, $p < 10^{-11}$). This result is
301 consistent with a convergence from OT into mTeg.

302 To test the prediction of covariation of preferred ITD and frequency in mTeg, we measured ITD
303 tuning in mTeg for tonal stimulation. As reported above, the ITD tuning curves of mTeg neurons
304 measured with tonal stimulation were sinusoidal functions with the period determined by the
305 stimulating frequency (Figure 2D,I). Remarkably, unlike in ICx and OT, where neurons prefer
306 the same ITD at all frequencies they respond to, i.e., they display a characteristic delay
307 (Takahashi and Konishi, 1986), mTeg neurons' preferred ITD varied with frequency (Figure
308 2I,J). For each cell, the peak ITD shifted towards 0 µs when the stimulus frequency increased
309 (Figure 2J, right, $r^2 = 0.85$, intercept=250 µs, slope= -0.042 µs/Hz, $p = 0.0019$). Moreover, the
310 relationship between preferred ITD and frequency in mTeg neurons matched the relationship
311 between preferred ITD and frequency in the space-map (Cazettes et al., 2014) ($r^2 = 0.75$,
312 intercept=284 µs, slope= -0.045 µs/Hz, $p<10^{-55}$), where frontal neurons, tuned to ITDs near zero,
313 prefer higher frequencies than peripheral neurons tuned to large ITDs (Figure 1) (Cazettes et al.,

314 2014; Knudsen, 1984). These results provide physiological evidence consistent with a
315 convergence from OT into mTeg.

316 **Weighted convergence from space-map to mTeg**

317 It was shown above that mTeg tuning to ITD and frequency are consistent with a convergence
318 that takes place between the space-map in OT and mTeg. We next asked whether the mTeg
319 responses can be explained by a weighted linear convergence from space-map neurons, a
320 processing scheme that has been proposed for the emergence of motor commands (Groh, 2001;
321 Salinas, 2006). For this, a bank of ITD tuning curves of a population of OT neurons was modeled
322 following criteria from published tuning properties of space-map neurons. Specifically, cells
323 tuned to frontal ITDs prefer higher frequencies and therefore display narrower ITD tuning
324 (Cazettes et al., 2014; Knudsen, 1984) (Figure 3A). This modeled OT population was the same
325 used previously for Bayesian decoding analyses (Cazettes et al., 2016). Modeled OT tuning
326 curves were then weighted (Figure 3B,C) and summed (Figure 3D) to simulate the weighted
327 convergence. To estimate the weights at each frequency/ITD channel converging onto mTeg
328 cells, we used linear decomposition by Fourier analysis of ITD tuning curves for broadband
329 noise of mTeg neurons. It has been shown that this method can be used to efficiently assess the
330 neurons' frequency responsiveness (Vonderschen and Wagner, 2012) (Figure 3B). Here, a higher
331 power at a specific frequency in the Fourier decomposition of the broadband-noise ITD response
332 of an mTeg neuron corresponds to a higher weight applied to the projecting OT neurons
333 corresponding to that frequency (Figure 3A-C). The weighted OT ITD-tuning curves were then
334 summed and the output was compared to the actual ITD tuning of mTeg neurons on a cell-by-
335 cell basis (Figure 3D). We observed strong correlations between modeled and measured mTeg
336 ITD-tuning curves (Figure 3E, pairwise linear correlation, $p<0.05$ for 34 out of 36 neurons,

337 median variance explained = 70%), indicating that ITD tuning of mTeg neurons to broadband
338 sound could be predicted from the weighted convergence of the space-map population. These
339 results indicate that mTeg responses are consistent with a weighted linear convergence from the
340 midbrain space map, a plausible mechanism in neural processing (Groh, 2001; Salinas, 2006).

341 **Emergence of an adaptive orientation estimate in mTeg**

342 We next examined whether mTeg responses predicted behavior when the reliability of the ITD
343 cue changed. To manipulate the reliability of the ITD cue, the similarity of the sound at the left
344 and right ears was varied by adding uncorrelated noise to reduce binaural correlation (BC).
345 Lowering BC increases the sensory noise. Previously reported data shows that the owl's
346 localization is increasingly biased toward zero degrees when BC decreases (Figure 4A,
347 reproduced from Saberi et al. (1998)). To compare the mTeg responses with the owl's
348 localization data, we plotted the mean mTeg responses as a function of BC for the same four
349 ITDs used in the published behavioral experiments. These mTeg responses were well correlated
350 with behavior (Figure 4B, mean r^2 for the four stimulus directions = 0.84, p=0.017).

351 Finally, we examined whether the bias in mTeg responses and the owl's behavioral bias matched
352 as BC changed. To compare the bias in mTeg responses and behavior we computed the mean
353 difference between responses at BC= 1 and at lower BCs (Figure 4C, D). The average mTeg
354 response predicted an increased bias at lower BCs (Figure 4D) that displayed a similar trend as
355 the orienting behavior of the owl (Figure 4C).

356 Overall, the correlation between mTeg neural responses and behavior across BCs supports the
357 hypothesis that mean mTeg responses approximate an estimate of sound direction that changes
358 adaptively when the sensory input is degraded.

359 **Testing the network architecture by manipulating the owl's behavioral bias**

360 To further test the weighted convergence model, we aimed to selectively manipulate the activity
361 in different parts of the space-map and verify whether these manipulations yielded consistent
362 changes in mTeg responses and the owl's behavior. Our hypotheses were based on previously
363 published evidence showing that frontal and peripheral space-map neurons are tuned to high and
364 low frequencies, respectively (Cazettes et al., 2014; Knudsen, 1984). Therefore, stimulation with
365 a sound containing only high frequencies should enhance the response of frontal space-map
366 neurons relative to peripheral neurons, with the converse occuring for stimulation with low
367 frequencies (Figure 5A). Hence, sound localizing behavior should display stronger bias for the
368 front for high-frequency than for low-frequency sounds. Moreover, if behavior is driven by the
369 mTeg responses, then the difference in mTeg responses to high and low frequency sounds should
370 match differences in behavioral localization bias for high and low frequency sounds.

371 To test whether the owl's behavioral bias was indeed consistent with these predictions, we
372 measured non-reinforced head-turns triggered by high and low-frequency band-pass as well as
373 broadband sounds in behaving barn owls. Training was limited to standing on a perch at the
374 center of a speaker array; in this way we avoided potential influences of over-training (Hazan et
375 al., 2015) (Figure 5B). The owl's natural tendency to orient the head toward sounds was tracked
376 with high-speed infrared cameras (Figure 5C). Head-saccades were measured from any initial
377 head angle to avoid positional biases. To control for the confound between centrality bias and
378 unwillingness of the barn owls to turn the head for sounds close to the center of gaze, sound
379 sources within 10 degrees or less from the center of gaze at the time of sound presentation were
380 not included in the analysis. We then estimated the average bias as the mean difference from the
381 actual sound source direction. Using this paradigm, owls underestimated peripheral directions for

broadband noise (the average bias over all eccentric directions was 21 deg), matching reports in previous studies using owls trained to fixate at the front and motivated to respond through reward (Hausmann et al., 2009; Knudsen et al., 1979). Remarkably, owls showed significantly stronger underestimation when localizing high frequency sounds than low frequency sounds ($p = 0.00004$, permutation test; average bias at high frequency: 27 deg; average bias at low frequency: 13 deg, see Figure 5D for the performance of each owl). Thus, the amount of behavioral bias could be adjusted upward and downward by targeted manipulations of the sensory input.

We then measured mTeg responses to the same high and low frequency sounds used in the behavioral experiments. We found that mTeg responses were consistent with the behavior, displaying significantly lower firing rate at peripheral ITDs for high than low frequencies (Figure 5E, $F(2,54) = 9.35$, $p = 0.0003$, ANCOVA). Specifically, the population mean mTeg response to ITD with high frequency sound was 30% lower than mTeg response to ITD with low frequency sound. In summary, the consistency between the mTeg neural responses and behavioral bias observed during stimulus' frequency manipulations indicates, independently from the BC manipulations, that mTeg responses could account for the behavioral bias by integrating across the space-map population.

DISCUSSION

This work provides evidence of how the midbrain map of auditory space may be read out by downstream neurons to synthesize a command of orienting behavior that captures sensory reliability. It has previously been shown that the selectivity of space-map neurons reflects cue reliability (Cazettes et al., 2014) and was proposed that this property may be a crucial parameter for guiding an adaptive behavioral bias (Cazettes et al., 2016). However, how exactly changes in space-map neurons' selectivity are translated into an adaptive behavior was left unanswered. The present study shows how the space-map population may be read-out by downstream neurons to guide behavior in situations of uncertainty. Here, we demonstrated that this processing is consistent with a weighted convergence from the OT to mTeg, generating a conversion from a map representation to a population rate-code that can drive orienting behavior in a manner that reflects sensory reliability. Based on these mechanistic findings, predictions were made about how the adaptive behavioral bias would change by controlling stimulus frequency. These predictions were confirmed with behavioral experiments, allowing further demonstration of the network architecture by manipulations at the encoding level. Therefore, we show here how sensory statistics can be biologically decoded into an adaptive signal controlling head saccade.

Sensory-motor integration

Critical findings of this study are the evidence of convergence from OT onto mTeg and the effect this convergence has on the ITD tuning in mTeg. Convergence from the space-map is supported by the broader frequency tuning of mTeg neurons and their frequency-dependent ITD tuning, which matches the ITD-dependent frequency tuning that was previously reported in ICx and OT (Cazettes et al., 2014; Knudsen, 1984). The remarkable consistency of how best ITD changes with frequency in mTeg with how best frequency changes with ITD in ICx (Cazettes et al., 2014)

423 and OT (Knudsen, 1984) indicates that convergent projections of neurons from the space-map
424 can explain the tuning in mTeg. As a consequence of this convergence, mTeg neurons lacked the
425 classic characteristic-delay described for neurons of the inferior colliculus (Takahashi and
426 Konishi, 1986). This is also consistent with the different ITD tuning of ICx and OT neurons,
427 compared to mTeg cells. Whereas ICx and OT responses display peaked and largely symmetric
428 rate-ITD curves around a prominent preferred ITD for broadband sound, mTeg responses are
429 largely asymmetric with maximal responses uniformly away from zero ITD.

430 A fundamental question in sensorimotor integration is the neural code controlling movement
431 (Todorov, 2000; Salinas, 2006; Overduin et al., 2012; Joshua and Lisberger, 2014). Previous
432 studies have reported correlations between the firing rate of sensorimotor neurons and the
433 kinematics of movements (Todorov, 2000). Here we propose that the premotor neurons in mTeg
434 encode direction in the population average firing rate, which, through weighted convergence,
435 captures the statistics of the sound localization cues that are represented in the upstream space-
436 map. This is consistent with the idea that mTeg neurons control muscle synergy rather than
437 single muscles independently (Masino and Knudsen, 1990; Overduin et al., 2012; Joshua and
438 Lisberger, 2014), which has been proposed for explaining why correlations between neuronal
439 responses and movement properties are commonly observed (Todorov, 2000).

440 The dorsal and medial tegmental areas are composed of multiple nuclei that receive direct
441 projections from the OT. Microstimulating these areas yields head-saccades in different
442 directions (Masino and Knudsen, 1993). Therefore, populations of mTeg neurons in distinct
443 nuclei are likely to have different tuning properties. Here, we focused on the horizontal
444 coordinate of sound direction, which in barn owls is specifically linked to the coding of ITD
445 (Moiseff, 1989). Hence, we targeted mTeg neurons with clear tuning to ITD throughout mTeg.

446 Because of the limited number of owls and the need to maximize the data collection, euthanasia
447 of birds used for recordings was not conducted, and we relied on physiological methods and
448 microstimulation to identify ITD-tuned mTeg cells. While the purpose of this study was to
449 elucidate the network underlying the emergence of an adaptive motor command for head
450 lateralization, we did not attempt to completely explain the anatomical pathway supporting head-
451 orienting responses. Further experiments are needed to explore the heterogeneous and likely
452 complex properties of mTeg neurons that participate in guiding eye and head movements in
453 different directions and contexts.

454 **Implementation of an adaptive behavior**

455 In general, behavioral errors are composed of systematic errors (biases) and precision errors
456 (variance). Previous studies have focused on behavioral biases to understand the underlying
457 neural code (Schwartz et al., 2007; Jazayeri and Shadlen, 2010; Summerfield and Lange, 2014;
458 Wei and Stocker, 2012, 2015). Focusing on the bias itself can provide information about the
459 strategy the brain uses to produce adaptive behavior. Although both bias and variance contribute
460 to the magnitude of errors, they provide different insights into how errors may occur in
461 judgments. While the variance may reflect the level of confidence in either the evidence or the
462 estimate, the systematic nature of the bias and its direction can be interpreted as the
463 manifestation of a prior (Fischer and Pena, 2011; Girshick et al., 2011; Cazettes et al., 2016; Wei
464 and Stocker, 2015) or a cost function (Kording and Wolpert, 2004) that constrains the judgment.
465 Understanding the neural response properties that emerge from the underlying circuitry in the
466 owl's sound localization pathway made it possible to manipulate the behavioral bias using
467 specific sensory stimuli. Thus a simple and biologically plausible mechanism of weighted
468 convergence can explain how the neural code for sound localization can be translated into an

adaptive behavioral command. These findings may also be testable in other species where auditory biases have been observed, including humans (Zahn et al., 1978; Populin and Yin, 1998; Nodal et al., 2008).

REFERENCES

Blauert J (1997) Spatial hearing: the psychophysics of human sound localization. Rev. edn, (MIT Press).

Cazettes F, Fischer BJ, Pena JL (2014) Spatial cue reliability drives frequency tuning in the Barn Owl's midbrain. eLife **3** doi:10.7554/eLife.04854.

Cazettes F, Fischer BJ, Pena JL (2016) Cue Reliability Represented in the Shape of Tuning Curves in the Owl's Sound Localization System. J Neurosci 36: 2101-2110.

du Lac S, Knudsen EI (1990) Neural maps of head movement vector and speed in the optic tectum of the barn owl. J Neurophysiol 63: 131-146.

Fischer BJ, Anderson CH, Pena JL (2009) Multiplicative auditory spatial receptive fields created by a hierarchy of population codes. PloS one 4: e8015, doi:10.1371/journal.pone.0008015.

Fischer BJ, Pena JL (2011) Owl's behavior and neural representation predicted by Bayesian inference. Nat Neurosci 14: 1061-1066.

Girshick AR, Landy MS, Simoncelli EP (2011) Cardinal rules: visual orientation perception reflects knowledge of environmental statistics. Nat Neurosci 14: 926-932.

Groh JM (2001) Converting neural signals from place codes to rate codes. Biol Cybern 85: 159-165.

490 Hausmann L, von Campenhausen M, Endler F, Singheiser M, Wagner H (2009) Improvements
491 of sound localization abilities by the facial ruff of the barn owl (Tyto alba) as demonstrated by
492 virtual ruff removal. PloS one 4: e7721, doi:10.1371/journal.pone.0007721.
493 Hazan Y, Kra Y, Yarin I, Wagner H, Gutfreund Y (2015) Visual-auditory integration for visual
494 search: a behavioral study in barn owls. Front Integ Neurosci 9: 11,
495 doi:10.3389/fnint.2015.00011.
496 Jazayeri M, Shadlen MN (2010) Temporal context calibrates interval timing. Nat Neurosci 13:
497 1020-1026.
498 Joshua M, Lisberger SG (2014) A framework for using signal, noise, and variation to determine
499 whether the brain controls movement synergies or single muscles. J Neurophysiol 111: 733-
500 745.
501 Knudsen EI (1982) Auditory and visual maps of space in the optic tectum of the owl. J Neurosci
502 2: 1177-1194.
503 Knudsen EI (1984) Auditory properties of space-tuned units in owl's optic tectum. J
504 Neurophysiol 52: 709-723.
505 Knudsen EI, Blasdel GG, Konishi M (1979) Mechanisms of sound localization in the barn owl
506 (Tyto alba). J Comp Physiol A 133: 13-21.
507 Knudsen EI, Knudsen PF (1983) Space-mapped auditory projections from the inferior colliculus
508 to the optic tectum in the barn owl (Tyto alba). J Comp Neurol 218: 187-196.
509 Knudsen EI, Konishi M (1978) A neural map of auditory space in the owl. Science 200: 795-
510 797.
511 Knudsen EI, Konishi M, Blasdel GG (1979) Sound Localization by the Barn Owl (Tyto alba)
512 measured with the Search Coil Technique. J. Comp. Physiol. 133: 1-11.

513 Koppl C (1997) Frequency tuning and spontaneous activity in the auditory nerve and cochlear
514 nucleus magnocellularis of the barn owl Tyto alba. J Neurophysiol **77**: 364-377.
515 Kording KP, Wolpert DM (2004) Bayesian integration in sensorimotor learning. Nature 427:
516 244-247.
517 Masino T (1992) Brainstem control of orienting movements: intrinsic coordinate systems and
518 underlying circuitry. Brain Behav Evol 40: 98-111.
519 Masino T, Knudsen EI (1990) Horizontal and vertical components of head movement are
520 controlled by distinct neural circuits in the barn owl. Nature 345: 434-437.
521 Masino T, Knudsen EI (1992) Anatomical pathways from the optic tectum to the spinal cord
522 subserving orienting movements in the barn owl. Exp Brain Res 92: 194-208.
523 Masino T, Knudsen EI (1993) Orienting head movements resulting from electrical
524 microstimulation of the brainstem tegmentum in the barn owl. J Neurosci 13: 351-370.
525 Moiseff A (1989) Bi-coordinate sound localization by the barn owl. J Comp Physiol A 164: 637-
526 644.
527 Mysore SP, Knudsen EI (2012) Reciprocal inhibition of inhibition: a circuit motif for flexible
528 categorization in stimulus selection. Neuron 73: 193-205.
529 Mysore SP, Knudsen EI (2014) Descending control of neural bias and selectivity in a spatial
530 attention network: rules and mechanisms. Neuron 84: 214-226.
531 Netser S, Ohayon S, Gutfreund Y (2010) Multiple manifestations of microstimulation in the
532 optic tectum: eye movements, pupil dilations, and sensory priming. J Neurophysiol 104: 108-
533 118.

534 Nodal FR, Bajo VM, Parsons CH, Schnupp JW, King AJ (2008) Sound localization behavior in
535 ferrets: comparison of acoustic orientation and approach-to-target responses. Neuroscience
536 154: 397-408.
537 Ohayon S, van der Willigen RF, Wagner H, Katsman I, Rivlin E (2006) On the barn owl's visual
538 pre-attack behavior: I. Structure of head movements and motion patterns. J Comp Physiol A
539 192: 927-940.
540 Olsen JF, Knudsen EI, Esterly SD (1989) Neural maps of interaural time and intensity
541 differences in the optic tectum of the barn owl. J Neurosci 9: 2591-2605.
542 Overduin SA, d'Avella A, Carmena JM, Bizzi E (2012) Microstimulation activates a handful of
543 muscle synergies. Neuron 76: 1071-1077.
544 Populin LC, Yin TC (1998) Behavioral studies of sound localization in the cat. J Neurosci 18:
545 2147-2160.
546 Rich D, Cazettes F, Wang Y, Pena JL, Fischer BJ (2015) Neural representation of probabilities
547 for Bayesian inference. J Comput Neurosci 38: 315-323.
548 Saberi K, Takahashi Y, Farahbod H, Konishi M (1999) Neural bases of an auditory illusion and
549 its elimination in owls. Nat Neurosci 2: 656-659.
550 Saberi K, Takahashi Y, Konishi M, Albeck Y, Arthur BJ, Farahbod H (1998) Effects of
551 interaural decorrelation on neural and behavioral detection of spatial cues. Neuron 21: 789-
552 798.
553 Salinas E (2006) How behavioral constraints may determine optimal sensory representations.
554 PLoS biology 4: e387, doi:10.1371/journal.pbio.0040387.

555 Schumacher JW, Schneider DM, Woolley SM (2011) Anesthetic state modulates excitability but
556 not spectral tuning or neural discrimination in single auditory midbrain neurons. J
557 Neurophysiol 106: 500-514.
558 Schwartz O, Hsu A, Dayan P (2007) Space and time in visual context. Nat Rev Neurosci 8: 522-
559 535.
560 Stocker AA, Simoncelli EP (2006) Noise characteristics and prior expectations in human visual
561 speed perception. Nat Neurosci 9: 578-585.
562 Strutt JW (1907) On our perception of sound direction. Philos Mag 13: 214-232.
563 Summerfield C, de Lange FP (2014) Expectation in perceptual decision making: neural and
564 computational mechanisms. Nat Rev Neurosci 15: 745-756.
565 Takahashi T, Konishi M (1986) Selectivity for interaural time difference in the owl's midbrain. J
566 Neurosci 6: 3413–3422.
567 Ter-Mikaelian M, Sanes DH, Semple MN (2007) Transformation of temporal properties between
568 auditory midbrain and cortex in the awake Mongolian gerbil. J Neurosci 27: 6091-6102.
569 Todorov E (2000) Direct cortical control of muscle activation in voluntary arm movements: a
570 model. Nat Neurosci 3: 391-398.
571 Vonderschen K, Wagner H (2012) Transformation from a pure time delay to a mixed time and
572 phase delay representation in the auditory forebrain pathway. J Neurosci 32: 5911-5923a.
573 Wang Y, Shanbhag SJ, Fischer BJ, Pena JL (2012) Population-wide bias of surround suppression
574 in auditory spatial receptive fields of the owl's midbrain. J Neurosci 32: 10470-10478.
575 Wei X, Stocker AA (2012) Bayesian inference with efficient neural population codes. In Proc Int
576 Conf on Artificial Neural Networks. NewYork: Springer.

Wei XX, Stocker AA (2015) A Bayesian observer model constrained by efficient coding can explain 'anti-Bayesian' percepts. Nat Neurosci 18: 1509-1517.

Weiss Y, Simoncelli EP, Adelson EH (2002) Motion illusions as optimal percepts. Nat Neurosci 5: 598-604.

Zahn JR, Abel LA, Dell'Osso LF (1978) Audio-ocular response characteristics. Sens Processes 2: 32-37.

584 **LEGENDS**

585 **Figure 1.** Sound localization pathway. ICx and OT display maps of frequency and space
586 (Knudsen, 1982; Cazettes et al. 2014). Frontal space (small ITD in µs in purple) is associated
587 with high frequency. Conversely, peripheral space (large ITD in µs in green) is associated with
588 low frequency. Although OT directly projects to mTeg, the nature of the projection between OT
589 and mTeg is unknown.

590 **Figure 2.** Tuning properties in the space-map and mTeg. (A) An eye tracking system detected
591 the pupil (blue ellipse) and the position of the corneal reflection (blue cross) over time. (B)
592 Microstimulation (red line) through the recording electrode elicited eye movements detected by
593 the eye tracker. (C,D) Example ITD tuning curves (mean and standard deviation across trials) of
594 ICx (C) and mTeg (D) neurons for tonal stimulation. (E,F) Example ITD tuning curves (mean
595 and standard deviation across trials) of ICx (E) and mTeg (F) neurons for broadband noise. (C-F:
596 mean and s.d.). (G) Evidence of frequency convergence from space-map to mTeg. Example
597 frequency tuning curve of an mTeg neuron (black) superimposed with frequency tuning curves
598 of ICx (green) and OT (blue) cells showing the broader frequency tuning in mTeg. (H) Across
599 the samples, mTeg neurons (n=36 from Owls #1, 2 & 3) were significantly more broadly tuned
600 than ICx (n=184 from Owls #1, 2 & 3) and OT (n=39 from Owls #4, 5 & 6) cells (Colored bar
601 represents median, box is 1st and 3rd quartiles, whiskers are 5 and 95%, crosses are greater than
602 95%, ***$p<0.001$). (I) Evidence of convergence across ITD channels from space-map to mTeg.
603 Example ITD tuning curves of an mTeg neuron for different frequencies, showing that ITD
604 tuning varied with frequency. (J) The mean and standard deviation of peak ITDs for tonal
605 stimulation across the mTeg sample. The mean peak ITD varied with stimulus frequency in a
606 manner consistent with how ITD and frequency tuning change in the space-map (Figure 1).

607 **Figure 3.** Weighted convergence from the space-map into mTeg. (A) Model of frequency-
608 dependent ITD tuning curves in the space map. Neurons tuned to small ITDs preferred high
609 frequencies (purple), neurons tuned to intermediate ITDs preferred intermediate frequencies
610 (blue) and neurons tuned to larger ITDs preferred low frequencies (green). (B) The weights for
611 each frequency (normalized from 0 to 1) were estimated from the Fourier decomposition of
612 responses of mTeg neurons to broadband sound, on a neuron-by-neuron basis. (C) Space-map
613 ITD tuning curves (A) scaled by the weights estimated in (B) and summed to simulate the
614 convergence. (D) Example experimental ITD-tuning curve in mTeg (gray dotted line) and the
615 output of the convergence model with the respective weights. (E) The boxplot shows the median
616 and quartiles of the coefficient of determination (r^2) between modeled and measured mTeg ITD
617 curves across the sample.

618 **Figure 4.** The owl's behavioral bias under varying levels of noise is consistent with mTeg
619 responses. (A) Mean and standard deviation of the owl's head orienting response as a function of
620 BC (modified from Saberi et al. 1998). Behavioral responses to four different ITDs are shown
621 (actual values indicated on the right). The centrality bias increases as BC decreases. (B) Mean
622 mTeg response across BC for similar ITDs as in (A). (C,D) Behavioral (C) and average mTeg
623 response changes as a function of BC, plotted as percent of the BC = 1 condition. To quantify the
624 bias toward the center in both behavior and neural responses, the mean difference between
625 responses at BC=1 and other BCs were computed at the same four directions shown in (A) and
626 (B). Error bars represent s.e.m.

627 **Figure 5.** Changes in the owl's behavioral bias and mTeg responses induced by manipulating
628 stimulus frequency. (A) Schematic population of space-map neurons whose relative response
629 rate varies with the frequency of the stimulating sound. Stimulation with high frequencies

630 (middle) excites more strongly the frontal neurons, which prefer higher frequencies. Conversely,
631 stimulation with low frequencies (bottom) excites more strongly the peripheral neurons. (B)
632 Owls were trained to stand on a perch at the center of a speaker array. (C) Images captured by
633 two high-speed infrared video cameras at different angles. The owl's head was tracked as it
634 moved in space. Red dotted lines indicate the trajectory preceding the shown images. (D) Mean
635 and s.e.m of the bias of head-orienting responses from three barn owls (F, L and P) presented
636 with high-frequency and low-frequency bandpass noise. (E) Mean ITD tuning across mTeg
637 neurons for low-frequency (green) and high-frequency (purple) bandpass noise.

638

ILLUSTRATIONS

Figure 1

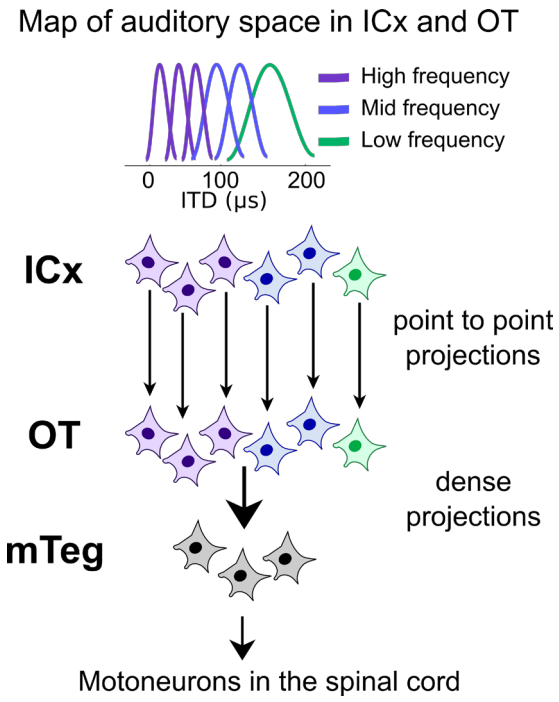

Sound localization pathway. ICx and OT display maps of frequency and space (Knudsen, 1982; Cazettes et al. 2014). Frontal space (small ITD in µs in purple) is associated with high frequency. Conversely, peripheral space (large ITD in µs in green) is associated with low frequency. Although OT directly projects to mTeg, the nature of the projection between OT and mTeg is unknown.

Figure 2

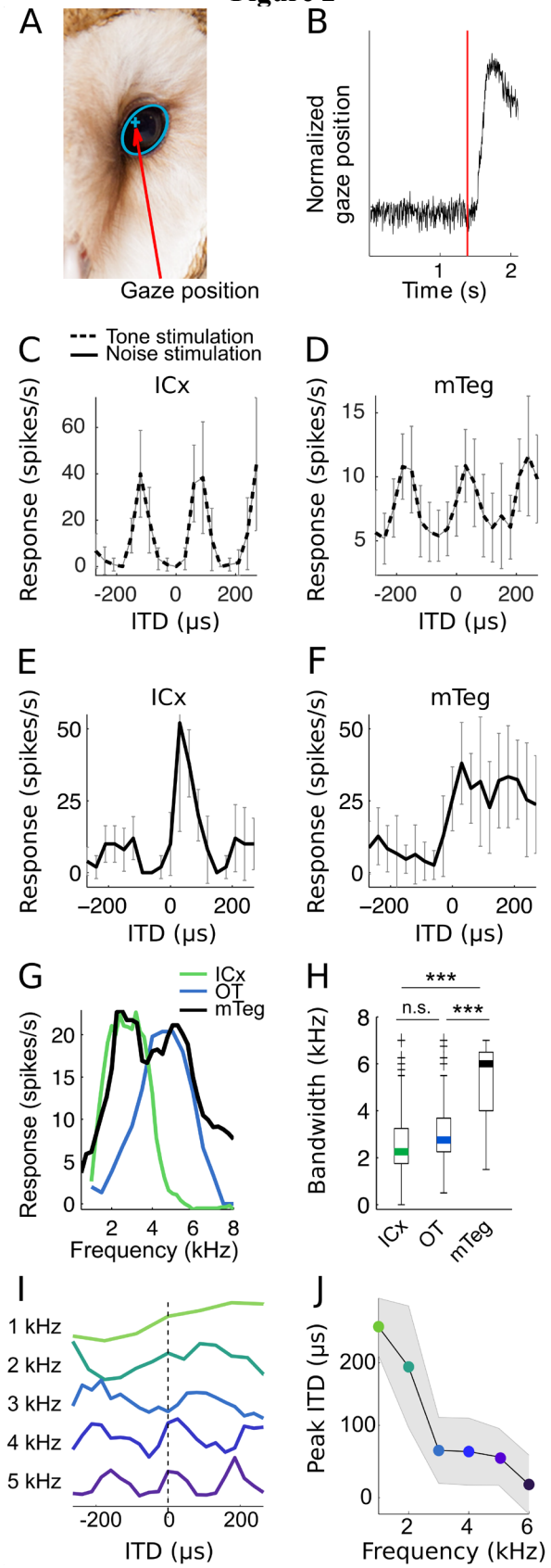
A
Gaze position
B
Normalized gaze position
Time (s)
C
Tone stimulation
Noise stimulation
ICx
Response (spikes/s)
ITD (μs)
D
mTeg
Response (spikes/s)
ITD (μs)
E
ICx
Response (spikes/s)
ITD (μs)
F
mTeg
Response (spikes/s)
ITD (μs)
G
ICx
OT
mTeg
Response (spikes/s)
Frequency (kHz)
H
***
n.s.
***
Bandwidth (kHz)
ICx
OT
mTeg
I
1 kHz
2 kHz
3 kHz
4 kHz
5 kHz
ITD (μs)
J
Peak ITD (μs)
Frequency (kHz)

652 Tuning properties in the space-map and mTeg. (A) An eye tracking system detected the pupil
653 (blue ellipse) and the position of the corneal reflection (blue cross) over time. (B)
654 Microstimulation (red line) through the recording electrode elicited eye movements detected by
655 the eye tracker. (C,D) Example ITD tuning curves (mean and standard deviation across trials) of
656 ICx (C) and mTeg (D) neurons for tonal stimulation. (E,F) Example ITD tuning curves (mean
657 and standard deviation across trials) of ICx (E) and mTeg (F) neurons for broadband noise. (C-F:
658 mean and s.d.). (G) Evidence of frequency convergence from space-map to mTeg. Example
659 frequency tuning curve of an mTeg neuron (black) superimposed with frequency tuning curves
660 of ICx (green) and OT (blue) cells showing the broader frequency tuning in mTeg. (H) Across
661 the samples, mTeg neurons (n=36 from Owls #1, 2 & 3) were significantly more broadly tuned
662 than ICx (n=184 from Owls #1, 2 & 3) and OT (n=39 from Owls #4, 5 & 6) cells (Colored bar
663 represents median, box is 1st and 3rd quartiles, whiskers are 5 and 95%, crosses are greater than
664 95%, ***$p<0.001$). (I) Evidence of convergence across ITD channels from space-map to mTeg.
665 Example ITD tuning curves of an mTeg neuron for different frequencies, showing that ITD
666 tuning varied with frequency. (J) The mean and standard deviation of peak ITDs for tonal
667 stimulation across the mTeg sample. The mean peak ITD varied with stimulus frequency in a
668 manner consistent with how ITD and frequency tuning change in the space-map (Figure 1).

669

Figure 3

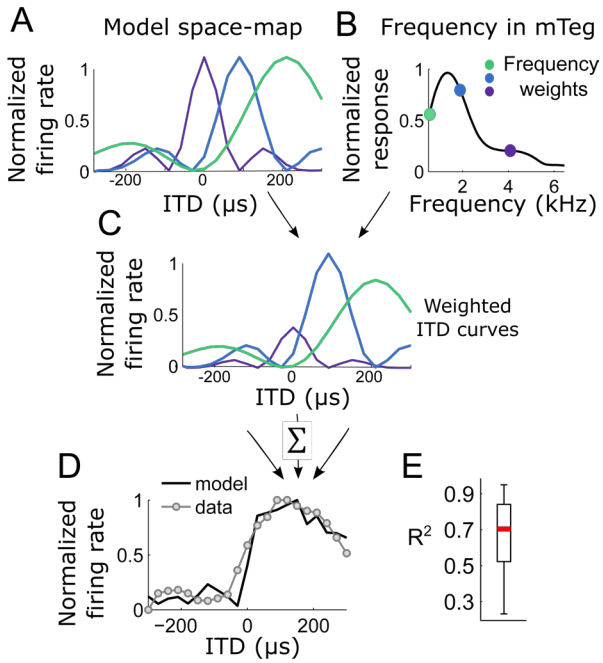

Weighted convergence from the space-map into mTeg. (A) Model of frequency-dependent ITD tuning curves in the space map. Neurons tuned to small ITDs preferred high frequencies (purple), neurons tuned to intermediate ITDs preferred intermediate frequencies (blue) and neurons tuned to larger ITDs preferred low frequencies (green). (B) The weights for each frequency (normalized from 0 to 1) were estimated from the Fourier decomposition of responses of mTeg neurons to broadband sound, on a neuron-by-neuron basis. (C) Space-map ITD tuning curves from A scaled by the weights estimated in B and summed to simulate the convergence. (D) Example experimental ITD-tuning curve in mTeg (gray dotted line) and the output of the convergence model with the respective weights. (E) Performance of the model in predicting the ITD tuning of mTeg neurons from their frequency tuning curves. The boxplot shows the median and quartiles and whiskers show 5% and 95% of the coefficient of determination (r^2) between modeled and measured mTeg ITD curves across the sample.

Figure 4

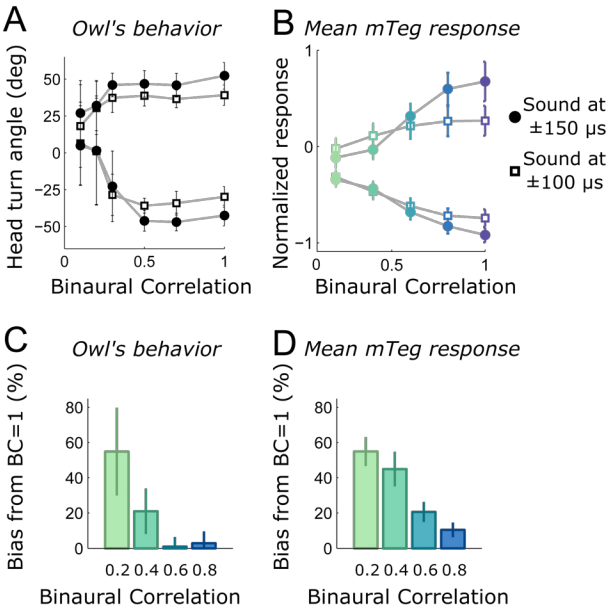

The owl's behavioral bias under varying levels of noise is consistent with mTeg responses. (A) The owl's head orienting response as a function of BC (modified from Saberi et al. 1998). Behavioral responses to four different ITDs are shown (actual values indicated on the right). The centrality bias increases as BC decreases. (B) Mean mTeg response across BC for similar ITDs as in A. (A-B plots display mean and stand deviation) (C,D) Behavioral (C) and average mTeg response (D) changes as a function of BC, plotted as percent of the BC = 1 condition. To quantify the bias toward the center in both behavior and neural responses, the mean difference between responses at BC=1 and other BCs were computed at the same four directions shown in A and B. (C-D Bars display mean and error bars represent s.e.m).

Figure 5

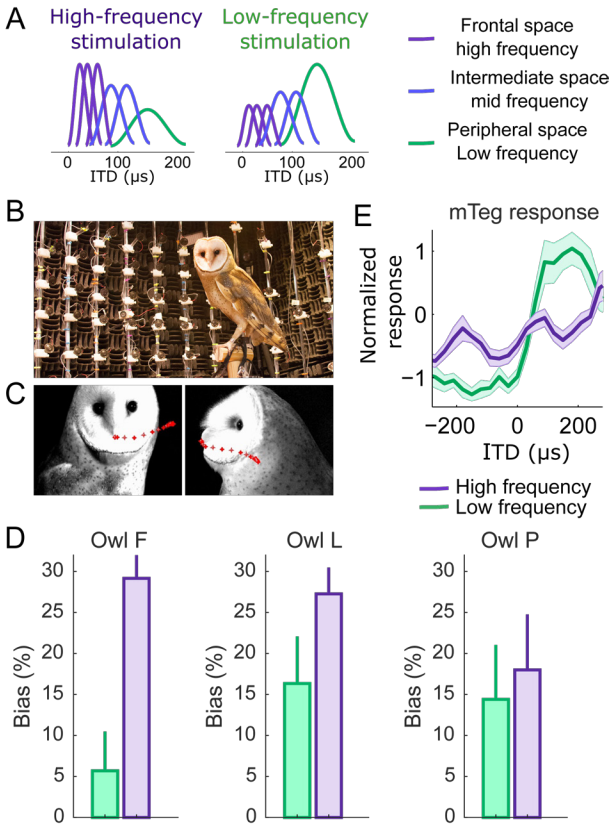

Changes in the owl's behavioral bias and mTeg responses induced by manipulating stimulus frequency. (A) Schematic population of space-map neurons whose relative response rate varies with the frequency of the stimulating sound. Stimulation with high frequencies (middle) excites more strongly the frontal neurons, which prefer higher frequencies. Conversely, stimulation with low frequencies (bottom) excites more strongly the peripheral neurons. (B) Owls were trained to stand on a perch at the center of a speaker array. (C) Images captured by two high-speed infrared video cameras at different angles. The owl’s head was tracked as it moved in space. Red dotted lines indicate the trajectory preceding the shown images. (D) Mean and s.e.m of the bias of head-orienting responses from three barn owls (F, L and P) presented with high-frequency and

710 low-frequency bandpass noise. (E) Mean ITD tuning and s.e.m across mTeg neurons for low-

711 frequency (green) and high-frequency (purple) bandpass noise.